VARIABLE PAST-REDOX CONDITIONS AT JEZERO CRATER, MARS. L. Mandon[1], B. L. Ehlmann[1], R. C. Wiens[2], B. Horgan[2], B. J. Garczynski[2], J. R. Johnson[3], E. Dehouck[4], C. Royer[2], T. Fouchet[5], J. I. Núñez[3], A. Brown[6] J. F. Bell III[7], S. Maurice[8]. [1]Caltech (lmandon@caltech.edu), [2]Purdue Univ., [3]JHUAPL, [4]LGLTPE, [5]LESIA, [6]Plancius Research [7]ASU, [8]IRAP.

Exploring a Martian paleolake: The Perseverance rover landed on Mars in 2021 in Jezero crater, an ancient lake. During the first 1.5 years of the mission, the rover investigated two geological units of the crater floor: the Máaz formation, interpreted to be lava flows of basaltic composition [1, 2], and the underlying Séítah formation, an olivine-rich cumulate [3]. Between sols ~420 and 640 (April to December 2022), Perseverance explored sedimentary terrains near the front of an ancient delta. The rocks at this location could have formed in various settings, including lacustrine, pro-deltaic or fluvial plain environments. Investigation of their mineralogy can yield information about the lake system and its watershed's past conditions, such as water availability, temperature, pH or redox states, which are keys to understand past-climate and habitability. Here, we expand on initial work [4] and compare the reflectance of rocks measured by the Mastcam-Z and SuperCam instruments to assess the variability of oxidized products along the stratigraphy. We focus on units well exposed at the delta front and with sufficient data, Amalik, Devils Tanyard, Hogwallow Flats (and lateral extension Yori Pass) and Rocky Top (stratigraphic relationships in Fig. 1) and compare their signatures to those of the igneous rocks of the crater floor.

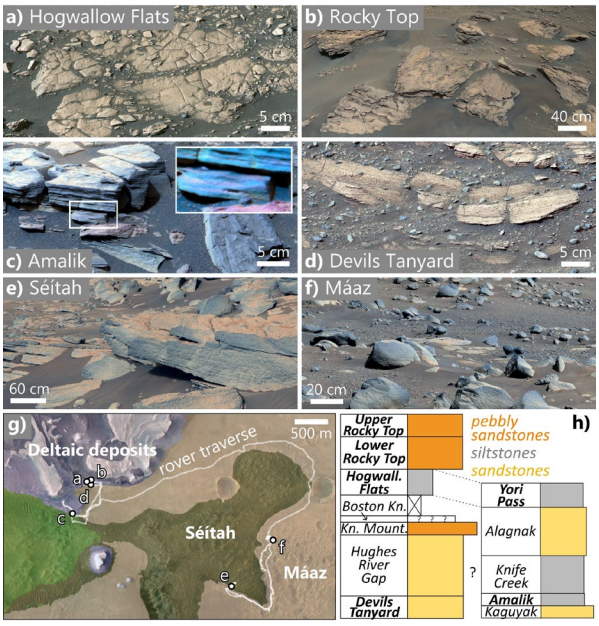

Fig. 1: (a-f) Mastcam-Z enhanced-color images of outcrops explored until sol ~620 (acquired on sols: (a) 502; (b) 492; (c) 423; (d) 449; (e) 211; (f) 78. **(g)** Geological map [12] over HiRISE basemap. **(h)** Stratigraphic relationship between the units explored during the delta front campaign and overlaying the crater floor igneous units.

Datasets: SuperCam's point spectrometer measures reflected light from 0.39 to 0.48 µm, 0.55 to 0.86 µm and 1.3 to 2.6 µm, enabling the identification of a wide variety of minerals, including mafic igneous minerals and secondary phases such as phyllosilicates, sulfates, or carbonates [5]. Mastcam-Z provides multispectral stereo-imaging with 12 narrowband filters centered in the 0.44-1.02 µm range, longer than the spectral range of SuperCam and including more Fe-oxide-related absorptions [6]. We used the data measured by the two instruments, calibrated to reflectance (processing described in [7, 8, 9]) and including division by cosine of solar incidence. For every combined observation of the same rock targets by the two instruments, we computed a mean spectrum of the SuperCam measurement (consisting of a raster of one to ten points) and extracted from the corresponding Mastcam-Z image an average spectrum from a region of interest (ROI) located at the same location. Discrepancies between the two instruments were possible from residual photometric effects owing to variable shadowing and/or acquisition times, distinct dust cover depending on whether the Mastcam-Z activity was performed before or after dust removal by a SuperCam's LIBS activity [4]. Although the spectral shapes were similar in most observations, an offset in reflectance was sometimes observed. Here, we focus on spectral shapes rather than absolute reflectance: in spectra shown here, Mastcam-Z data was normalized to SuperCam spectra at 0.63 µm.

Color and spectral variation of rocks (Figs. 2 and 3)**:** Spectra of the Séítah igneous rocks show a deep 0.7-1.8 µm absorption related to olivine [8]. Least dusty surfaces exhibit positive but moderate 0.53 µm band depths, consistent with the small amounts of ferric oxides (e.g., ferrihydrite) suggested by [8]. Spectra of the Máaz igneous rocks absorb more deeply at 0.53 µm and have a broad, shallow absorption at ~0.9 µm, also consistent with the Fe^{3+}-oxyhydroxides, pyroxenes and feldspars detected by [8, 10]. Sedimentary rocks are more variable in Fe-related and H_2O/OH-related absorptions. Amalik rocks are overall dark in the visible ($R^* < 0.2$) and have flat spectra in the 0.6-0.9 µm range, indicating a strong visible absorber such as an opaque mineral or mixed valence oxide (e.g., magnetite). A relatively strong slope in the 1.3-1.8 µm range suggests ferrous material. Banding of more and less red material (Fig. 1c, increased saturation inset) suggest variability of Fe oxidation at the scale of the Amalik outcrop. Weak 1.9 µm and sharp 2.33 µm absorptions indicate the

presence of a poorly hydrated Mg-phyllosilicate, possibly a serpentine [11] or chlorite. By contrast with Amalik, the Devils Tanyard, Hogwallow Flats and Rocky Top members all exhibit deeper hydration bands near 1.4 and 1.9 µm and stronger Fe^{3+}-related absorptions compared to Máaz, Séítah, and Amalik. Devils Tanyard is highly oxidized: the rocks are redder than the other subunits, with deep 0.53 µm and 0.86 µm absorptions, indicative of crystalline hematite. Fe/Mg-phyllosilicates are detected (absorptions at 1.4, 1.9, 2.3 and 2.4 µm [11]). An absorption centered at 2.30 µm indicates less Fe^{3+} as the dominant octahedral cation, compared to the Máaz formation where it is centered at 2.28 µm, characteristic of dominantly Fe^{3+} nontronite. The Hogwallow Flats rock spectra are broadly flat in the 0.9-1.8 µm range, pointing towards low content of ferrous material. In the visible range, they are highly variable. In some spectra, an absorption centered at ~0.86 µm indicates a ferric phase; a coupled sharp absorption at 0.43 µm [13] and drop-off after 2.3 µm suggest that this phase is a sulfate, although some abraded surfaces at the top of the unit exhibit stronger 0.53 µm bands, making the presence of crystalline hematite also possible. Crystalline ferric oxides also seem to be present in the Rocky Top member, which exhibits relatively strong 0.53 µm and 0.86 µm absorptions. A reflectance drop-off past 0.9 µm points towards the presence of a ferrous phase as well.

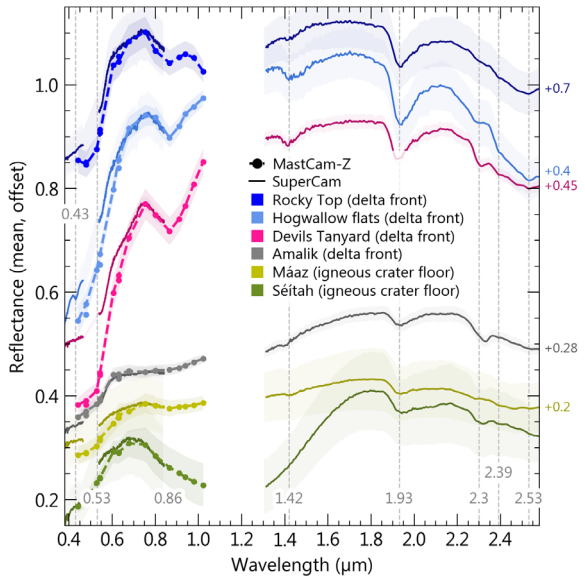

Fig. 2: Reflectance of abraded rocks, averaged by unit type (± std).

Oxidized intervals in Jezero stratigraphy: A small amount of Fe^{3+}-oxyhydroxides and Fe^{3+}-phyllosilicates are associated with the igneous units. More significant amount of Fe^{3+}-oxides and Fe^{3+}-sulfates occur in the overlying delta front sediments. The latter also show water-related features, indicative of more interaction of water with the sedimentary rocks comprising the delta compared to the igneous floor rocks. Over the few tens of meters of stratigraphy explored near the delta front, Fe is observed in different redox states, e.g., spectroscopically, the Devils Tanyard member is oxidized while the darkest portions of the Amalik member are mostly ferrous. At Hogwallow Flats, rocks at the top of the unit are more oxidized than at the bottom. From observations so far, it is unclear whether spectral indicators of redox variability within and between the units are related to a difference of redox conditions during the deposition of these materials, to unequal burial and exposure to oxidative weathering, or to source rocks of different composition. At Amalik, redox variations are seen at the cm-scale, without variation of composition or grain size at ~50 µm/pixel. This suggests possibly periodical control of redox conditions during deposition (possibly induced by lake levels fluctuations, groundwater infiltration and/or change of atmospheric composition [14, 15]), rather than diagenesis. Future work will expand on refining the water chemistry of the lake to assess these scenarios.

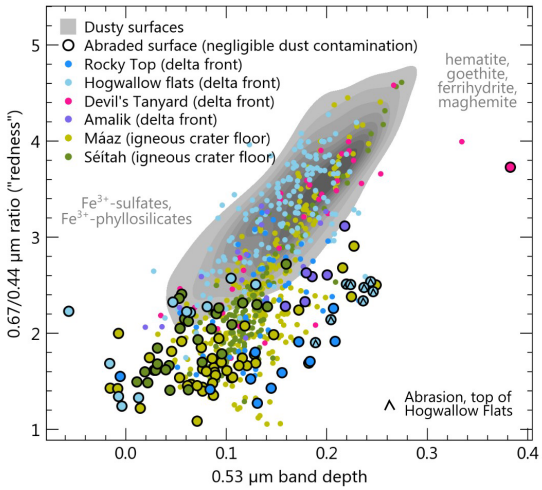

Fig. 3: Mastcam-Z 0.67/0.44 µm ratio and 0.53 µm band depth of ROIs collected from rock observations. These values of these parameters for ROIs on dusty surfaces are shown as a kernel density representing 90% of the distribution.

References: [1] Wiens et al (2022) *Sci. Adv.* 8; [2] Udry et al. (2023) *JGR: Plan.*; [3] Liu et al. (2022) *Science* 377; [4] Johnson et al. (2022) *53th LPSC*; [5] Maurice et al. (2021) *Space Sci. Rev.* 217; [6] Bell et al. (2021) 217; [7] Merusi et al. (2023) *JGR: Plan.*; [8] Mandon et al. (2023) *JGR: Plan.*; [9] Royer et al. (2023) *JGR: Plan.*; [10] Horgan et al. (in rev.); [11] Dehouck et al. *this conf.*; [12] Stack et al. (2020) *Space Sci. Rev.* 216; [13] Johnson, J. R. et al., *this conf.* ; [14] Hurowitz et al. (2017) *Science.* 356; [15] Wordsworth et al. (2021) *Nat. Geo.* 14.